Langmuir

Article

pubs.acs.org/Langmuir

Molecular Dynamics Simulation of Water/BHDC Cationic Reverse Micelles. Structural Characterization, Dynamical Properties, and Influence of Solvent on Intermicellar Interactions

Federico M. Agazzi,[†] N. Mariano Correa,[†] and Javier Rodriguez*[,§,#]

[†]Departamento de Química, Universidad Nacional de Río Cuarto, Agencia Postal 3, C.P. X5804BYA Río Cuarto, Argentina

[§]Departamento de Física de la Materia Condensada, Comisión Nacional de Energía Atómica, Avenida Libertador 8250, 1429 Buenos Aires, Argentina

[#]ECyT, UNSAM, Martín de Irigoyen 3100, 1650 San Martín, Provincia de Buenos Aires, Argentina

Supporting Information

ABSTRACT: We report results obtained from molecular dynamics (MD) experiments of benzylhexadecyldimethylammonium chloride (BHDC) cationic reverse micelles (RMs). In particular we analyzed equilibrium and dynamical characteristics of water/BHDC RMs in pure benzene, at two different water/BHDC ratios (W_0 = 5 and W_0 = 10). The RMs appear as elliptical aggregates with eccentricities close to ∼0.9. Analysis of the different spatial correlations reveals three different spatial domains in the RMs: a water inner pool, the surfactant interface, and the external solvent. The calculated accessible surface areas for the aqueous inner cores suggest a strong penetration of solvent molecules within the micellar interface domains. Comparison between the density profiles of both RMs shows an increment of the broadness in the distributions of all species at the interface, along with an increasing overlap between the tail segments of the surfactant and benzene molecules as one considers larger micelles. For the dynamical side, the rotational characteristic time scale for the confined water was found to be 1 order of magnitude larger than that of the bulk water. A similar effect was also observed for hydrogen bond dynamics. Both retardation effects diminish with the size of the aggregate. To the estimate the influence of the external solvent on the intermicellar interactions, free energy profiles for the coalescence process between RMs of similar size in pure benzene and in a *n*-heptane/benzene mixture were also investigated. The results indicate that the association process is facilitated by the presence of *n*-heptane in the external nonpolar phase. Comparison with previous theoretical and experimental results is also carried out.

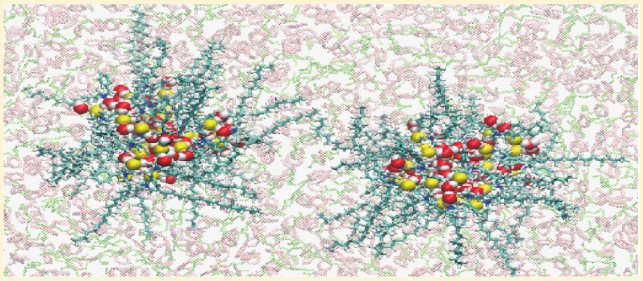

1. INTRODUCTION

Reverse micelles (RMs) are commonly described as highly structured, supramolecular systems built by the self-assembly of surfactant species dispersed in a nonpolar medium. A third polar component can be encapsulated within the micellar structure, leading to the formation of an inner pool of nanometer dimensions, surrounded by the headgroups of the surfactants. RMs have been the subject of a wide variety of experimental studies since the early 1940s.[1] Depending on the characteristics of the surfactants, the list includes nonionic, anionic, and cationic detergents paired with different polar solvents. Due to the large diversity of microenvironments that these materials provide, RMs have found a wide range of applications in different areas of chemical, biological, and material sciences.[2,3]

The nature of the encapsulated solvent also makes it possible to discriminate between aqueous[4] and nonaqueous[5] RMs. To characterize aqueous RMs, it is useful to introduce a quantitative parameter, W_0, which is frequently associated with the micellar size and defined in terms of the ratio between the molar concentrations of water and surfactant:

$$W_0 = \frac{[\text{water}]}{[\text{surfactant}]} \quad (1)$$

Most of the experimental studies concerning RMs have analyzed the behavior of the anionic surfactant AOT (sodium 1,4-bis-2-ethylhexyl sulfosuccinate), in different nonpolar solvents.[4,6] On the other hand, the analyses of cationic RMs have been mostly performed in systems composed by quaternary aliphatic ammonium salts, such as cetyltrimethylammonium bromide (CTAB).[7−9] Nevertheless, in this paper we will focus our attention on a less employed cationic surfactant: benzylhexadecyldimethylammonium chloride (BHDC) (Figure 1a).[10−14] Until recent years, the BHDC surfactant had been employed only to produce RMs dispersed

Received: May 20, 2014
Revised: July 23, 2014
Published: July 28, 2014

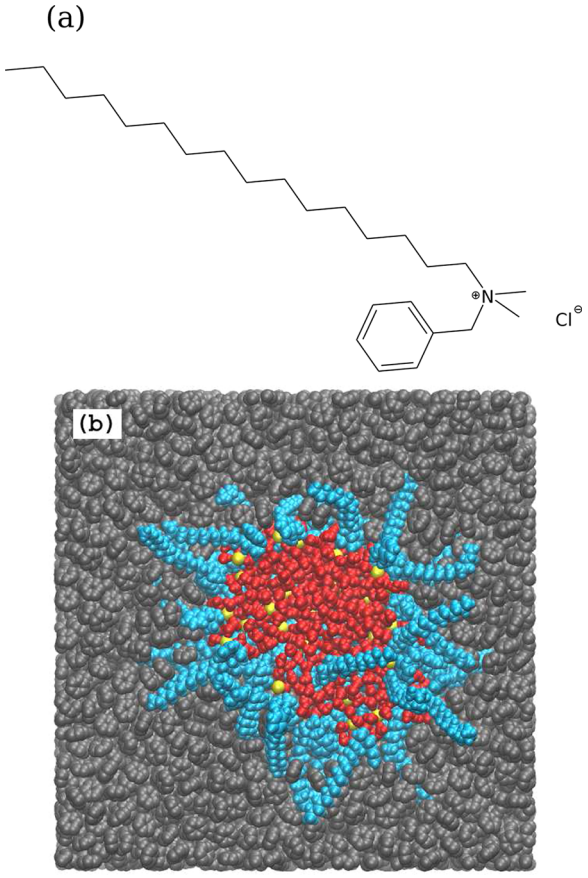

Figure 1. (a) Molecular structure of BHDC surfactant. (b) View of RM10 system across the $z = 0$ plane of the simulation box. The red, yellow, and cyan colors correspond to water molecules, chloride ions, and BHD^+ moieties, respectively. The benzene molecules are rendered in gray.

in pure aromatic solvents, such as benzene. Compared to water/AOT RMs, the water/BHDC RMs were seldom studied. The experimental methodologies applied for their characterization include IR spectroscopy,[10] nuclear magnetic resonance (NMR),[10] dynamic light scattering (DLS),[13] and absorption and emission spectroscopy.[10−14] For example, Jada et al.[11] investigated different cationic RMs, including one composed of water/BHDC in benzene, by means of time-resolved fluorescence quenching, light scattering, and electrical conductivity. They found that, for a given cationic surfactant, the aggregation number and the material exchange rate constant between droplets increase with W_0. Moreover, they also verified the disappearance of phase percolation for micelles with high W_0. The authors rationalized these observations in terms of a stiffening of the interface due to a significant folding of BHDC tails as the size of the aggregates increases. Correa et al.[4] analyzed the local polarity of different environments within water/BHDC RM in benzene. Their spectroscopy experiments revealed the complete hydration of the ionic head surfactant for $W_0 \geq 10$. Moreover, they also found that, even at the maximum experimentally accessible value of W_0, the polarity sensed by the spectroscopic probe at the confined pool never reaches the value observed in pure water. In a related context, Quintana et al.[12] have investigated the behavior of the cationic hemicyanine (HC) in water/BHDC RMs in benzene, using absorption and emission spectroscopy techniques. Their results suggest a reduction in the "electron-donor character" of the water molecules trapped inside the BHDC RMs. More recent studies performed in our group[13,14] have shown that water/BHDC RMs can also be stabilized in mixtures of *n*-heptane/benzene. At a given W_0, we observed that the droplet sizes increase as the proportion of *n*-heptane in the solution increases. On the other hand, the local polarity of the environment and the magnitude of the water−surfactant coupling were found to change dramatically with the composition of the nonpolar phase, a result that was rationalized by taking into account the magnitude of the solvent penetration into the interface and its influence over both the droplet−droplet interaction and the water structure inside the RMs. For the practical application of RMs as nanoreactors,[15−19] it was found that one of the key steps that controls the synthetic pathway is the coalescence process, which is regulated by intermicellar interactions. Despite their importance, the intermicellar interactions and the coalescence of RMs have been rarely studied.[13,20−25] Indeed, none of these works have analyzed the influence of the external nonpolar solvent on the effective interaction between RMs.

The works mentioned above have provided elements pertaining to the macroscopic description of water/BHDC RMs in benzene and have relied exclusively on the direct interpretation of the experimental signals. Despite the rich variety of behaviors, a microscopic description of the different microenvironments is still lacking. In this context, computer simulation appears to be a suitable tool to gain a complementary description of these micellar systems at the atomic level. Several computational studies has been performed to analyze nonionic isolated RMs[26−29] and AOT RM.[30−39] These works have employed different modeling schemes, ranging from mean field approximations to coarse-grained and fully atomistic descriptions of the systems under investigation. In what follows, we will present results from the computer simulation of BHDC RMs. In particular, we focused attention on the following: (i) We studied different structural and dynamics properties of the water/BHDC/benzene RMs at $W_0 = 5$ and 10. In all cases, we established comparisons between the behaviors of encapsulated and bulk water. Furthermore, we compared the properties determined in the present molecular dynamics (MD) study to those previously obtained in our group for similar systems.[13,14] Despite the difference between BHDC and AOT molecular structures, and due to the lack of MD experiments devoted to the study of cationic RMs, a comparison between water/BHDC RMs properties and water/AOT anionic RMs characteristics studied by computer simulation was also carried out.[30−39] (ii) We determined free energy profiles for the coalescence processes between water/BHDC RMs with similar size, immersed in different external nonpolar phases. In addition, we obtained a molecular description of the effects derived from the presence of this nonpolar solvent on the fusion process.

This paper is structured as follows: in section 2, we describe the model and the simulation procedure; section 3 contains the main results of the MD simulations; and in section 4 we summarize the main conclusions of the paper.

2. MODEL AND SIMULATION DETAILS

Two different RMs corresponding to water/BHDC/benzene systems were investigated: a $W_0 = 5$ (labeled RM5) and a $W_0 = 10$ (labeled RM10). Both systems have been well characterized by experimental measurements.[13,14] The preparation of each system involved a six-step

dx.doi.org/10.1021/la501964q | Langmuir 2014, 30, 9643−9653

procedure, the details of which can be found in the Supporting Information.

To investigate the influence of the external solvent on the properties of the micellar interface, a third system was analyzed. This system, labeled RM2, is composed of water/BHDC RMs with a W_0 = 2 dispersed in a *n*-heptane/benzene mixture with an *n*-heptane molar fraction X_{Hp} = 0.30. Table 1 summarizes the relevant parameters concerning sizes and compositions of the simulated RMs.

Table 1. Detailed Sizes and Compositions of RM5, RM10, and RM2 Systems[a]

system	W_0	R (Å)	N_w	N_{BHDC}	N_{Bz}	N_{Hp}	L (Å)
RM5	5	30	60	12	3338	0	80
RM10	10	40	700	70	6085	0	100
RM2	2	32.5	60	30	1962	843	80

[a]R corresponds to the experimental hydrodynamics radius reported in a previous work.[13] N_w, N_{BHDC}, N_{Bz}, and N_{Hp} represent the number of water, BHDC, benzene, and *n*-heptane molecules, respectively. L corresponds to the simulation box length. For the free energy experiments, a rectangular simulation box of dimensions $L_z = 2L_y = 2L_x = 2L$ was employed; consequently, the sizes of the systems were duplicated.

All different components were modeled as a collection of interacting sites. As usual, the overall potential energy of the system included a sum of site−site, pairwise interactions combining dispersion (Lennard-Jones) and Coulomb contributions. The intermolecular and intramolecular interactions of BHDC molecules were modeled using the all-atom CHARMM27 force field.[40] Water was described by the SPC/E model.[41,42] To describe benzene and *n*-heptane a united-atom model[43] was employed to reduce computational costs. It is important to note that to validate this solvent representation, complementary MD experiments with a fully atomistic description of benzene and *n*-heptane molecules were also performed, and no significant discrepancies between results obtained from either modeling scheme were observed.

MD trajectories correspond to the NVT ensemble. The average temperature was set to 298 K and the average pressure to ∼1 bar. The NVT runs lasted, typically, 40 ns. Statistical averages of all relevant observables were calculated using the last 30 ns portions of the trajectories. Along these runs, the overall shapes of the RMs looked fairly stable. The trajectories were generated using the NAMD software package.[44] A Langevin thermostat was applied. The time step was set at 1 fs, and the long-range force arising from Coulomb interactions was treated using a particle-mesh Ewald sum procedure.[45,46] The equations of motion were integrated using a multiple time-step integration scheme, with a time step of 1 fs for intramolecular modes and nonbonded short-range forces and of 2 fs for the rest of the Coulomb forces. To estimate the effect of the RM confinement over water properties, benchmark experiments of bulk water were performed in the NVT ensemble at the same thermodynamic conditions.

The Helmholtz free energy profiles for the coalescence process between micelles were calculated using the adaptive biasing force (ABF) scheme,[47] as implemented in the NAMD code. This methodology relies on the generation of trajectories along a chosen reaction coordinate ξ, experiencing practically no free energy barriers. This is achieved by a biasing force estimated along a series of small bins, which, in turn, span the complete ξ interval. The net force along the ξ coordinate is practically zero, and the evolution of the system along this reaction coordinate is mainly governed by self-diffusion properties. In this case the chosen reaction coordinate ξ was the distance between the centers of mass of the two RMs. Additional technical details concerning the procedure are summarized as follows: (i) the free energy profile was obtained by dividing the ξ interval into 3 Å wide overlapping windows; (ii) to keep the intermicellar axis along the z direction, a confining harmonic potential was applied over the centers of mass of the micelles along the x and y directions, with constants $k_{x-y} \sim 0.05$ kcal mol^{-1} Å^{-2}; (iii) within each window, instantaneous values of the forces were harvested in 0.1 Å bins. Convergence within each window typically required a sequence of ∼2 × 10^6 simulations steps.

3. RESULTS AND DISCUSSION

3.1. Shape and Size of the Reverse Micelles. We will first focus attention on the overall shape of the simulated RMs. Figure 1b shows a snapshot of a typical configuration of RM10, obtained from an equilibrium trajectory. Similar results were obtained for the RM5 system (not shown). Although RMs are highly complex geometrical objects, their overall shapes can still be conveniently approximated by an ellipsoid. Thus, for each point of the MD trajectories we determined the three semiaxes a, b, and c from the equations

$$I_1 = \frac{1}{5}M(a^2 + b^2)$$
$$I_2 = \frac{1}{5}M(a^2 + c^2)$$
$$I_3 = \frac{1}{5}M(b^2 + c^2) \quad (2)$$

where $I_1 > I_2 > I_3$ are the principal moments of inertia of the RM and M represents its total mass. In this context, a relevant order parameter to characterize the shape of the RM is given by the micellar eccentricity, e, defined as

$$e = \sqrt{1 - \frac{c^2}{a^2}} \quad (3)$$

Note that, for a spherical-like object, e is near zero, whereas $e \rightarrow 1$ for ellipsoidal shapes.[32,48]

In Figure 2a, typical evolutions for the eccentricity of the water core and of the total RM for the RM10 system are shown. Similar behavior was obtained for RM5 (not shown). In the first rows of Table 2, we list average values for the semiaxes and the calculated eccentricities for the RMs analyzed. The superscripts "w", in RM5^w and RM10^w, denote averages taken over water molecules exclusively. Data corresponding to labels RM5 and RM10 were calculated considering the complete micellar system.

The calculated eccentricities, $e \sim 0.8$−-0.9, reveal that water/BHDC/benzene RMs can be reasonably well described as triaxial elliptical aggregates. Similar deviations from the spherical shape have been found in previous simulation works dealing with anionic AOT RMs.[32−34,38,39,48] Comparison between the values reported in these studies and those presented here shows that cationic RMs present higher eccentricities than those observed in anionic micelles of similar size. This observation could be ascribed to effects derived from differences in the external solvent employed in these experiments and their influence on the surfactant packing at the RM interface.

At this point it will be instructive to compare experimental results previously obtained in our group and the computer simulation observations presented above. In a previous work,[13] we studied the formation of water/BHDC/benzene RMs using DLS. We observed a linear relationship between the W_0 value and the droplet size, expressed in terms of the apparent hydrodynamics radius (R_H) of the aggregate. In earlier works,[32,49] this linear trend was also derived by assuming

dx.doi.org/10.1021/la501964q | Langmuir 2014, 30, 9643−9653

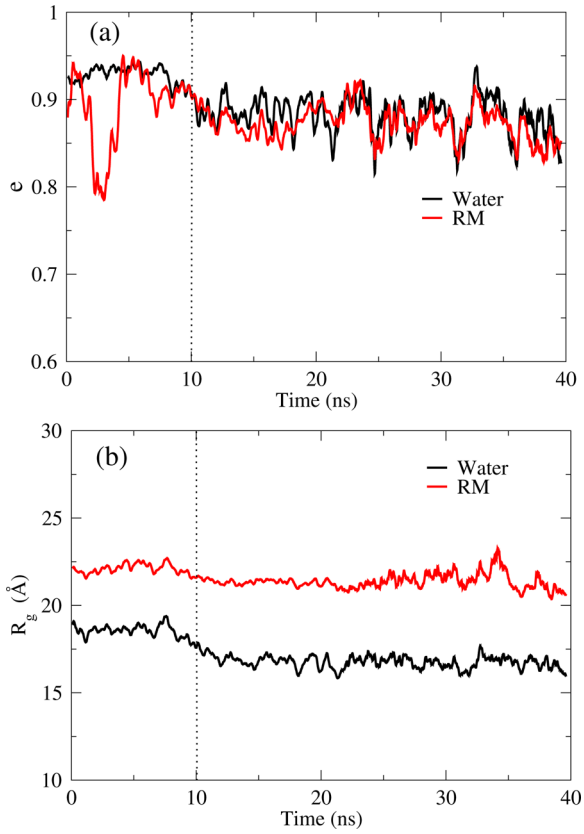

Figure 2. Evolution of (a) eccentricity e and (b) radius of gyration R_g for RM10. The black (red) line corresponds to the water core (complete RM). The dotted line indicates the initial time from which statistical information was harvested.

Table 2. Average Values of the Semiaxes (a, b, and c), Eccentricity (e), Radius of Gyration (R_g), Experimental Hydrodynamics Radius (R_H), and Normalized Accessible Surface Areas for BHDC Surfactants (ASA_{BHDC}) and Water Pool (ASA_w) for RM5 and RM10[a]

	RM5[w]	RM5	RM10[w]	RM10
$\langle a \rangle$	11.65	20.73	27.20	34.24
$\langle b \rangle$	9.69	14.18	22.35	28.21
$\langle c \rangle$	7.73	10.41	12.57	16.65
$\langle e \rangle$	0.73	0.86	0.87	0.88
$\langle R_g \rangle$	7.63	12.19	16.79	21.21
R_H		30[b]		40[b]
$\langle ASA_{BHDC} \rangle$	0.90		0.64	
$\langle ASA_w \rangle$	0.10		0.36	

[a]All length parameters are expressed in Å.The superscript "w" indicates that only the water molecules were considered for the calculations. [b]Reference 13.

overall spherical shapes for the water pools of RMs with radius equal to R^w_{sph}, that is

$$R^w_{sph} = \frac{3v_w}{a_s}W_0 + \frac{3v_s}{a_s} \quad (4)$$

where v_w is the "volume" of a water molecule, a_s is the area per surfactant headgroup, and v_s represents the volume of the water-penetrated portion of a surfactant headgroup.[32]

In the Supporting Information we show that these linear trends can also be obtained for the case of an ellipsoidal aggregate. In these cases, eq 4 can be rewritten as

$$R^w_e \approx \frac{v_w}{a_s}F \qquad W_0 + \frac{v_s}{a_s}F \quad (5)$$

where F represents a geometric factor depending on the semiaxis values. If one assumes that the geometric factor F does not change significantly with W_0, a linear relationship between the radius of the aqueous core and W_0 should be expected for an ellipsoidal water pool as well.

On the other hand, if the hydrodynamic radius is approximated by

$$R_H \approx R^w_e + l_{eff} \quad (6)$$

where l_{eff} is the effective thickness of nonpolar regions at the micellar interface (including tails of surfactant and benzene molecules), the linear relationship previously reported is regained:

$$R_H \approx \frac{v_w}{a_s}F \qquad W_0 + \frac{v_s}{a_s}F + l_{eff} \quad (7)$$

We calculated the geometric factor F for each RM from the semiaxis values reported in Table 2 and, in both cases, we found values close to $F \approx 3$. This confirms that the referred linear trend should be expected even for elliptical symmetries if a homogeneous growth of the RMs with W_0 is observed.

On the other hand, the RM size can be estimated from the radius of gyration (R_g) of the RM, defined as

$$R_g = \sqrt{\frac{\sum_i m_i r_i^2}{\sum_i m_i}} \quad (8)$$

where m_i is the mass of atom i located at radial distance r_i from the center of mass of the RM. Figure 2b shows a typical evolution of the radius of gyration for the water core and the entire RM for the RM10 system. Similar behaviors were obtained for RM5 (not shown). In Table 2, we present results obtained for the average radius of gyration for the RMs analyzed. Some features deserve comment. Size observables obtained from our MD experiments (expressed in terms of R_g) and those determined in our previous work by DLS experiments (expressed by R_H) show similar dependence on W_0.[13] However, as expected, R_H values are larger than R_g values for RM5 and RM10 systems. Note that the experimental R_H values are calculated from the diffusion coefficients of the RMs, assuming a spherical shape for the aggregate and neglecting effects related to the presence of solvent molecules associated with the external domain of the RM. On the other hand, in our MD experiments, micellar sizes were estimated by focusing exclusively on the water and BHDC molecules that comprise the system, without any a priori assumptions about the overall shapes of the aggregates.

The calculation of the differences between R_g values for the entire RM and the water pool provides rough estimates for the thickness of the surfactant layer. For the two RMs, these differences correspond to approximately 5 Å and could be ascribed to two main facts: (i) the significant folding of hydrocarbon tails of BHDC (note that the length of the hydrophobic chain in its extended conformation is about ≈20 Å) and (ii) the penetration of water molecules into the hydrophobic region of BHDC. These two observations are in

dx.doi.org/10.1021/la501964q | Langmuir 2014, 30, 9643−9653

accordance with results from experiments made in BHDC RMs[11] and for MD simulation of AOT RMs.[32]

3.2. Surface Characterization. To gain insights about the surface characteristics of RMs, the accessible surface areas (ASAs) for the BHDC (ASA_{BHDC}) and for the inner of water pool (ASA_w) were determined. Calculations of the ASA parameter were carried out by implementing the NSOL algorithm.[50] In Table 2, we present results for ⟨ASA⟩. The reported areas were normalized so that $\langle ASA_{BHDC}\rangle + \langle ASA_w\rangle = 1$.

The magnitude of $\langle ASA_w\rangle$ values obtained for both systems is of the order of 10−40% of the total exposed area and reveals significant contact between the water core and the external solvent. The strong interpenetration between the two domains is the result of an interplay between the spatial arrangement adopted by the surfactants at the RMs interface and the geometrical characteristics of the benzene molecules. As such, our results contrast sharply with those obtained by Abel et al. for water/AOT/isooctane RMs at W_0 = 3, 5, and 7.[32] In the latter case, $\langle ASA_w\rangle$ values were close to zero, suggesting a negligible penetration of isooctane molecules inside the hydrophilic region of the AOT RMs. Steric effects may be invoked to explain these different behaviors: (i) AOT is a two-tailed surfactant and, therefore, the effective volume of the hydrophobic region is larger than that for micelles comprising BHDC surfactants, precluding the penetration of the solvent; (ii) on the other hand, isooctane molecules are larger and more flexible than the planar and more rigid benzene moieties. As a result, the incorporation of solvent into the AOT RM interface should be disfavored. Moreover, as W_0 and the size of the RM increase, the solvent−water contact increases by a factor of ∼4. This would be indicative of a less efficient packing of the BHDC surfactants, as W_0 increases. Consequently, the penetrations of the external solvent and the inner water domain into the micellar interface go hand in hand with the micellar size.

3.3. Density Profiles. The microscopic structure of the inhomogeneous RMs can be described by the local density fields associated with a set of relevant chemical species. A reasonable choice for the origin of the reference system is the position of the center of mass of the RM ($\mathbf{r}_{CM}$). Density profiles can be calculated from

$$\rho_\alpha = \frac{1}{4\pi r^2}\sum_i \langle \delta(|\mathbf{r}_i^\alpha - \mathbf{r}_{CM}| - r)\rangle \tag{9}$$

In this equation, ⟨...⟩ denotes an equilibrium ensemble average, whereas $\mathbf{r}_i^\alpha$ represents the coordinate of the ith site of molecule α.

In Figure 3 we present the density profiles for RM5 and RM10. The curves correspond to the following species: water oxygen, chloride, center of mass of benzene, nitrogen atoms located at the BHDC headgroups. and the set of carbon atoms comprising the hydrophobic tails of the surfactants. The insets in this figure show additional information about density profiles for the following species: methyl groups, nitrogen atoms, benzyl group. and hydrocarbon tails for RM5 and RM10 systems. It is worth commenting that the nonspherical shape of the RMs restricts the interpretation of these, presumed spherically, symmetric radial distribution functions. Despite these limitations, we believe that the interpretation of these profiles is instructive.[36] At a first glance, one can distinguish three spatial domains: (i) an inner core, for $r \lesssim 7$ Å ($r \lesssim 15$ Å) for RM5

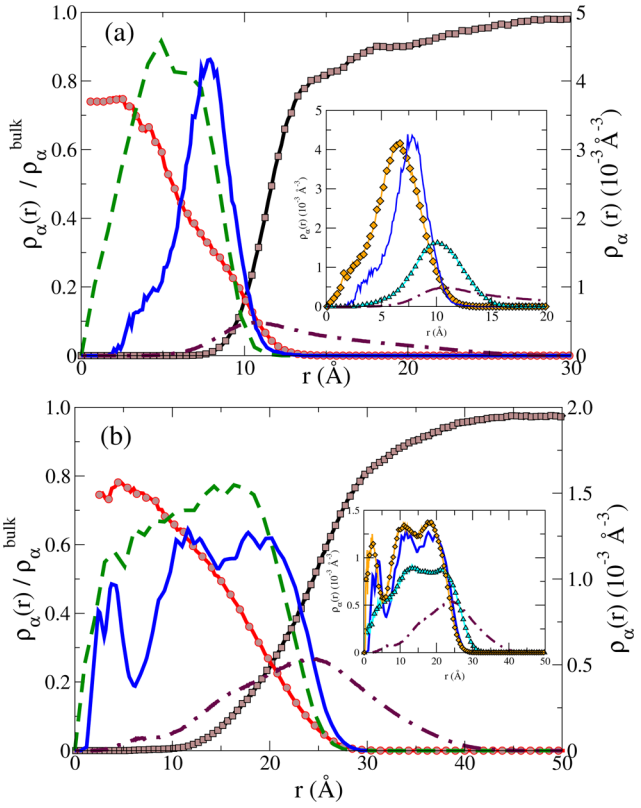

Figure 3. Density profiles for RM5 (a) and RM10 (b), corresponding to water oxygens (circles-line), chloride ions (dashed line), nitrogen sites (solid line), all sites of the hydrocarbon tails (dot-dashed line), and centers of mass of benzene molecules (squares-line). Water oxygen and benzene density profiles are normalized with respect to the corresponding bulk densities (left y-axis). The insets in panel a show the density profiles of methyl groups (diamonds-line), nitrogen stes (solid line), benzyl group (triangles-line), and all sites of the hydrocarbon tails (dot-dashed line).

(RM10), where water prevails; (ii) an interfacial region, primarily occupied by BHDC surfactants, that spans along the 7 Å $\lesssim r \lesssim$ 20 Å (15 Å $\lesssim r \lesssim$ 35 Å) interval for RM5 (RM10); and (iii) the nonpolar, external phase of benzene, located at distances $r \gtrsim$ 20 Å ($r \gtrsim$ 35 Å) for RM5 (RM10). A more detailed analysis of the density profiles reveals additional information: (i) In both RMs, the water in the core reaches a maximum density that is ∼80% of its bulk value. Similar results were reported for water/AOT RMs.[32,36] This reduction may be due to the strong hydration of the ionic headgroups and to the seepage of water into the hydrophobic region. (ii) For the RM5, the Cl^- density profile shows a sharp peak, located at $r \approx$ 5 Å, adjacent to the nitrogen peak at $r \approx$ 7 Å. On the other hand, in RM10, the Cl^- profile looks broader, revealing a large spatial delocalization all across the water pool. This result would indicate that the combined effect of confinement and Coulomb coupling leads to stronger spatial localization of these ionic species, the smaller the size of the RM considered. (iii) The main peak of the BHDC nitrogen profile also looks sharper in smaller micelles. In addition, as the micelle size increases, this density profile also looks broader and turns multimodal, a fact that could be ascribed to the presence of less structured interface. Note that a secondary peak for the N density profile can be observed at $r \approx$ 4 Å, revealing that some hydrophilic headgroups of BHDC molecules protrude into the water pool domain. (iv) The density profile for benzene exhibits significant

dx.doi.org/10.1021/la501964q | Langmuir 2014, 30, 9643−9653

overlaps with those corresponding to BHDC tails and water. This observation agrees with experimental results obtained by our work group[13,14] and reinforces our previous interpretations concerning the $\langle ASA_w \rangle$ values and the penetrations of the external solvent within the micellar interface. (v) The inset in Figure 3 shows that the methyl groups in the BHDC headgroups are oriented toward the water micellar core, whereas the benzyl moieties lie within the interfacial domain, closer to the surfactant chains and the nonpolar solvent molecules. This observation agrees with the experimental results presented by McNeil et al.[10]

The nonspherical shape of the RMs and the roughness of their interfaces certainly smooth the local density profiles presented above. To minimize these effects, intrinsic density profiles of water and benzene, referred to the nitrogen atom of the BHDC surfactant head, were calculated according to the tesselation procedure proposed by Chowdhary et al.[36] Intrinsic density profiles for RM5 and RM10 are shown in Figure 4. The

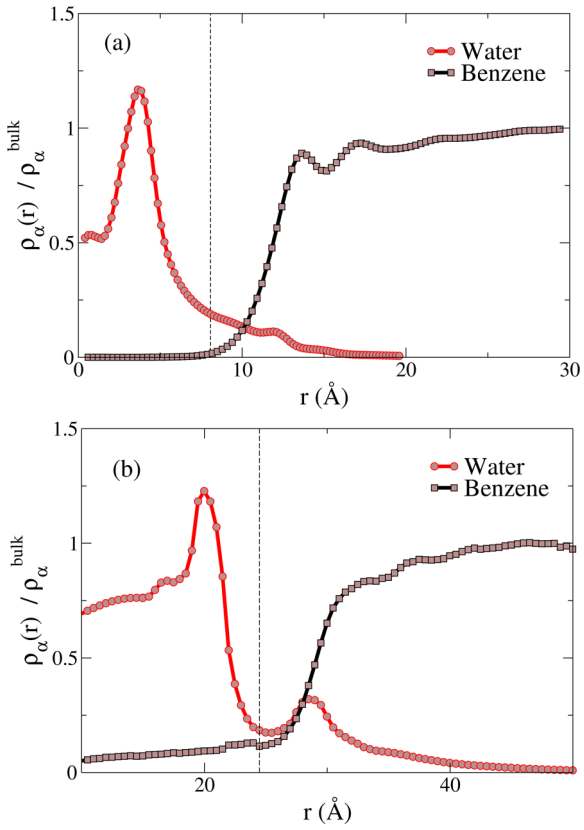

Figure 4. Intrinsic density profiles for RM5 (a) and RM10 (b), corresponding to water oxygens (circles-line) and centers of mass of benzene molecules (squares-line). Water oxygen and benzene density profiles are normalized with respect to the corresponding bulk densities. The dashed line indicates the average distance between nitrogen sites and the center of mass of the micelle.

marked enhancement of the water density observed at the polar region of the RM reveals the strong solvation of the BHDC head by the water molecules located at the inner portion of the RM. Additionally, it is noted that some of the water molecules of this first solvation shell can protrude into the apolar phase (note, for instance, the presence of a local maximum located at $r \approx 30$ Å for RM10). The joint analysis of both panels reveals the increment of the overlap between water and benzene phases with the size of the aggregate, in accordance with the previous observations.

3.4. Solvation of the Charged Moieties. To gain insights about the structural characteristic of the water pool, we have computed pair densities between water oxygen sites and nitrogen atoms at the surfactant heads and chloride anions, respectively. Pair densities are defined as

$$\rho_{\alpha\beta}(r) = \frac{1}{N_i 4\pi r^2} \sum_i \sum_{j \neq i} \langle \delta(|\mathbf{r}_i^\alpha - \mathbf{r}_j^\beta| - r) \rangle \quad (10)$$

Figure 5 shows the local oxygen densities around Cl^- anions and N sites for the two systems analyzed. In both RMs, the

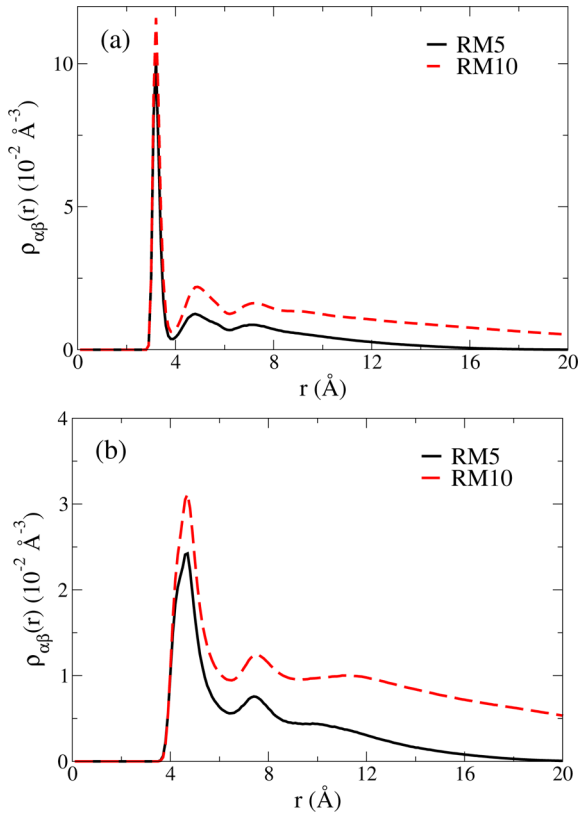

Figure 5. Correlation density functions for the (a) Cl^-−O and (b) N−O pairs in RM5 and RM10.

solvation profile of Cl^- is characterized by the presence of three maxima, the prominent one being at $r \approx 3.9$ Å. Integration of $\rho_{\alpha\beta}(r)$ over this first peak reveals that the first solvation shells of Cl^- are composed of approximately $N_w \approx 5$ water molecules, contrasting with $N_w \approx 6$ found for the bulk water.[51,52]

On the other hand, the solvation profile of nitrogen in the BHDC is also characterized by the presence of three peaks, with a prominent maximum located at $r \approx 4.5$ Å. The number of nearest neighbors is 10 (15) for RM5 (RM10) micelles, showing that the degree of hydration of the BHDC headgroups increases with the micellar size. Similar behaviors were reported for water/AOT anionic RMs.[32−34,36]

A comparison between the pair densities shows that the first peak for N−O looks smaller and wider than that for Cl−O, most likely due to the presence of the bulkier methyl groups that prevents a close approach of the solvent to the N site.

3.5. Rotational Dynamics. In the next two sections, we will examine the dynamical properties of water molecules

dx.doi.org/10.1021/la501964q | Langmuir 2014, 30, 9643−9653

located within the micellar core. To that end, we will first focus attention on the water rotational dynamics by analyzing time correlation functions of the type

$$C_\mu(t) = \langle P_1[\hat{\boldsymbol{\mu}}_i(t)\cdot\hat{\boldsymbol{\mu}}_i(0)]\rangle \quad (11)$$

where $P_1(x) = x$ corresponds to the first-order Legendre polynomial and $\hat{\boldsymbol{\mu}}_i$ represents a unit vector along the direction of the dipolar moment of the tagged molecule of water. In Figure 6a, we display results for $C_\mu(t)$ in bulk and in RMs. To obtain a qualitative estimate of the overall effects on the water dynamics, in Table 3 results for τ_{rot}, the time integral of $C_\mu(t)$, are also listed.

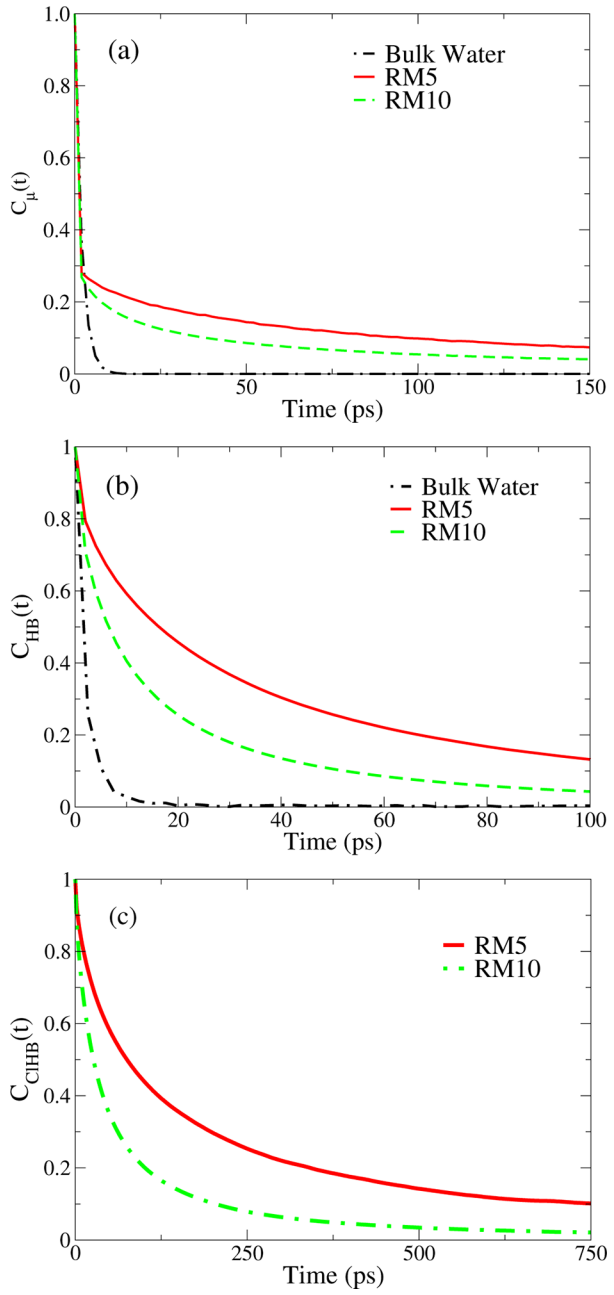

Figure 6. (a) Single−dipole time correlation function, $C_\mu(t)$ and (b) survival probability function, $C_{HB}(t)$, for hydrogen bonds in water for RM5 and RM10. The correlation functions for bulk water are also displayed. (c) Survival probability function, $C_{ClHB}(t)$, for hydrogen bonds between water and chloride anions in RM5 and RM10.

Table 3. Average Reorientational Times (Calculated from Time Integrals of $C_\mu(t)$) and Intermittent Hydrogen Bond Lifetimes (Calculated from Time Integrals of $C_{HB}(t)$) for Water Molecules in RM5, RM10, and Bulk Water, Respectively[a]

Water		
system	τ_{rot} (ps)	τ_{HB} (ps)
RM5	43.1	53.3
RM10	23.2	23.5
bulk water	3.12	4.60

Chloride−Water				
system	a_1	τ_1 (ps)	a_2	τ_2 (ps)
RM5	0.68	63	0.32	714
RM10	0.70	25	0.30	213

[a]Constants corresponding to biexponential fitting of $C_{ClHB}(t)$ for hydrogen bond dynamics between water and chloride anions in RM5 and RM10.

Compared to the bulk results, the profiles of $C_\mu(t)$ for both RMs exhibit slower decays, the τ_{rot} values being 1 order of magnitude larger than those in the macroscopic phase. Furthermore, the value of τ_{rot} in RM5 system is approximately 2 times larger than the corresponding one for RM10. Combined effects of confinement and electrostatic coupling can be invoked to rationalize this slowdown in the dynamics of water.[31,32,37,48,53−55] Moreover, the dependence of τ_{rot} on the micellar size can be explained on the basis of basic stoichiometric arguments: (i) The amount of water permeating within the RM5 interface domain is smaller, which leads to an effective higher concentration ratio [BHDC]/[H_2O]. (ii) Ionic concentration in the water pool of the RM scales as W_0^{-1}. Consequently in RM5, water molecules are necessarily subjected to stronger Coulombic couplings.

In passing, it is also instructive to establish a comparison between the present data and the value τ_{rot} = 98 ps reported by Pomata et al. for W_0 = 7 water/AOT RMs.[48] In the latter case the slower water rotational dynamics observed is likely due to the stronger hydrogen bonds established between water and oxygen sulfonate anions of the surfactant headgroups.

3.6. Hydrogen Bond Dynamics. To analyze hydrogen bonding (HB) dynamics, we computed the time correlation function

$$C_{HB}(t) = \sum_{ij} \frac{\langle h_{ij}(t)h_{ij}(0)\rangle}{\langle h_{ij}(0)^2\rangle} \quad (12)$$

where $h_{ij}(t)$ = 1 if molecules i and j are H bonded at time t and 0 otherwise, assuming the intermittent approximation.[48,56−58] Our definition of HB was based on the geometric criterion described in ref 59, which establishes that a pair of water molecules is considered to be hydrogen bonded if the O−O distance is smaller than 3.5 Å and the O−O−H angle is smaller than 30°. Results for $C_{HB}(t)$ are shown in Figure 6b. To perform a comparative analysis between the different systems, we estimated the mean lifetimes (τ_{HB}) from time integrals of $C_{HB}(t)$.[57] The results are listed in column 3 of Table 3. In accordance with results reported for the rotational dynamics, the values of τ_{HB} for micellar systems are about 1 order of magnitude larger than corresponding ones observed in the macroscopic phase, the variation of τ_{HB} being of similar order to the one reported for τ_{rot}. Furthermore, τ_{HB} for RM5 approximately doubles the value obtained for RM10. As a

dx.doi.org/10.1021/la501964q | Langmuir 2014, 30, 9643−9653

possible explanation for these similarities it is important to keep in mind that the same effects that cause alterations on the translational and rotational mobilities of water molecules will also affect the HB dynamics. In RMs, a significant number of water molecules protrudes into the interfacial domains. For these water molecules, the slower translational and rotational mobilities necessarily stretch HB lifetimes. Similarly to what has been described for the case of rotational dynamics, the slowdown in the HB dynamics in the water pool could be associated with the increment in the Coulombic coupling that, in turn, would bring additional rigidity to the overall architecture of HBs.

Finally, the analysis of the hydrogen bond dynamics between water and chloride ions (ClHB) was performed. For these calculations, the geometrical criteria previously employed for the definition of the HB were modified, setting the cutoff HB distance between Cl^- ions and water oxygens to 4 Å. Results of the corresponding time correlation functions are shown in Figure 6c. The $C_{ClHB}(t)$ profiles could be adequately fitted by biexponential functions of the type

$$C_{ClHB}(t) \approx \sum_{i=1}^{2} a_i \exp(-t/\tau_i) \quad (13)$$

Decays for RM5 and RM10 can be reasonably well described by involving two different time scales: the fast initial decorrelation, τ_1, of some tens of picoseconds, and a a second, somewhat slower, stage characterized by τ_2, of the order of a few hundreds of picoseconds. The corresponding fitting constants are listed in Table 3. As observed for the other dynamical parameters, both RM5 time scales are about ∼2−3 times larger than the RM10 corresponding ones, the fast components of the ClHB decays being of the same order of magnitude as τ_{HB} and τ_{rot}. Additionaly, an increment of ∼3−6 times is observed when τ_1 is compared to the reported values of HB relaxation times of bulk solutions of chloride.[60]

3.7. Intermicellar Interactions. To complete our analysis we will examine the influence of the external solvent on the intermicellar interactions and the coalescence process. Effective intermicellar interactions were investigated by computing free energy profiles associated with the coalescence process between two RMs of similar size. Two different kinds of water/BHDC RMs were studied: (i) the RM5 dispersed in pure benzene, that is, X_{Hp} = 0.00, and (ii) RMs with W_0 = 2 (RM2) in a *n*-heptane/benzene mixture with X_{Hp} = 0.30. These RMs were chosen to minimize the influence of the micellar dimensions over the intermicellar interaction, based on the experimental size data reported previously.[13]

In our analysis, we adopted a simple geometrical order parameter to gauge the degree of advance of the coalescence process (ξ) defined as the z component of the vector that separates the centers of mass of the two RMs:

$$\xi = Z_A - Z_B \quad (14)$$

In Figure 7 we present results for $\Delta A = A(\xi) - A(\xi = \infty)$, obtained using the ABF scheme. In the free energy plot of RM5, some characteristic features can be singled out. As one moves from larger to shorter intermicellar separations, one observes the following: (i) A first secondary maximum of the order of ∼5 kcal/mol at $\xi \approx 60$ Å corresponds to the loss of the more distant solvation shell of the RMs. (ii) Alocal minimum at $\xi \approx 50$ Å is ascribed to a more favorable reaccommodation of a surrounding solvation shell. (iii) A shoulder, clearly detected at

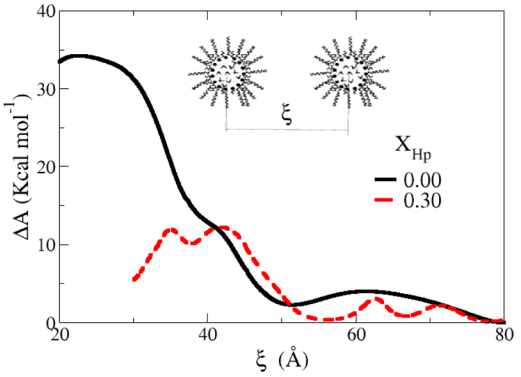

Figure 7. Helmholtz free energy profiles for the coalescence process of the reverse micelles in benzene (X_{Hp} = 0.00) and *n*-heptane/benzene mixture (X_{Hp} = 0.30).

$\xi \approx 40$ Å, matches twice the radius of gyration of each RM and would represent a "contact distance". It can be argued that below this threshold distance, a new set of forces originated by the direct interaction between segments of surfactant tails will control the progression of the coalescence mechanism. However, these tail−tail interactions are not the only driving agents for the approaching process. To make this point clear, in Figure 8a we present axial local density profiles of some relevant species along the intermicellar axis for X_{Hp} = 0.00 at $\xi \approx 40$ Å, computed as

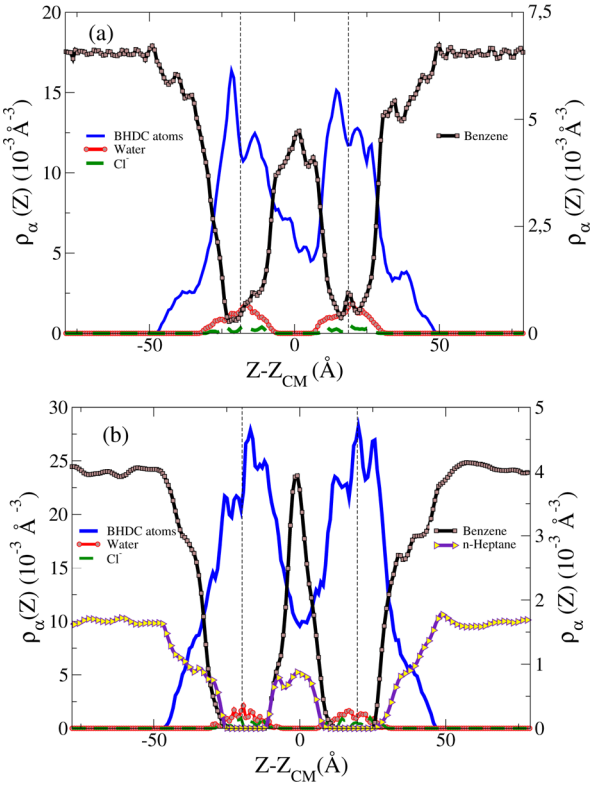

Figure 8. Density profiles along Z for (a) RMs with X_{Hp} = 0.00 and for (b) RMs with X_{Hp} = 0.30, corresponding to water oxygens (circles-line), chloride ions (dashed line), BHDC atoms (solid line), centers of mass of benzene molecules (squares-line, left y-axis), and centers of mass of *n*-heptane molecules (triangles right-line, left y-axis). The dashed line indicates the positions of center of mass for each RM.

dx.doi.org/10.1021/la501964q | *Langmuir* 2014, 30, 9643−9653

$$\rho_\alpha(z) = \frac{1}{\pi R_g^2} \sum_i \langle \delta(z_i^\alpha - Z_{CM} - z) \rangle \quad (15)$$

where z_i^α is the z-coordinate of the ith site in the molecule of species α, Z_{CM} is the center of mass of the micellar system, and R_g is the radius of gyration of the corresponding single micelle. The obtained value for the density ratio $\rho^{Bz}_{intermicellar}/\rho^{Bz}_{external} \approx 0.75$ reveals the presence of a significant amount of solvent molecules within the intermicellar region. We tend to believe that the subsequent and abrupt rise of the energy for $\xi \lesssim 35$ Å could also be associated with the irreversible work necessary to release these tightly trapped molecules. (iv) Finally, a high energy barrier of the order of $\Delta A_{Bz} \approx 35$ kcal/mol located at $\xi \approx 25$ Å is observed. Below this distance, interpenetration between the micelle cores and rearrangement of water molecules via the formation of new hydrogen bonds finally drive the system into the global minimum (not shown).

Interestingly, the energy profile for the RM2 system contrasts sharply: (i) not only one, as in the case of RM5, but two local maxima can be observed at long separations ($\xi \approx 65$ Å); (ii) a few angstroms below the "contact distance", and after surpassing an energy barrier of $\Delta A_{mix} \approx 12$ kcal/mol, the system stabilizes at a local minimum ($\xi \approx 38$ Å); (iii) at even smaller distances, the free energy profile shows a steady drop toward the global minimum. As a net result, the overall free energy barrier is, in this case, of the order of one-third of ΔA_{Bz}.

In Figure 8b the density profile $\rho_\alpha(z)$ for $X_{Hp} = 0.30$ at $\xi \approx 40$ Å is also shown. Note that, although the ratio $\rho^{Bz}_{intermicellar}/\rho^{Bz}_{external}$ is close to ~1, for *n*-heptane the relationship $\rho^{Hp}_{intermicellar}/\rho^{Hp}_{external}$ comes close to ~0.5, revealing the more uneasy packing of the aliphatic solvent within the surfactant tails. Consequently, we tend to believe that the reduction of *n*-heptane molecules in the intermicellar region could facilitate the association process between RMs. The decrease of the effective free energy barrier previously described clearly indicates that the association process "benefits" from the presence of *n*-heptane in the solvent mixture.

It is well established that intermicellar attractions are mainly controlled by solvent removal from the overlapping regions and its transfer to the bulk.[20,22] Therefore, we are led to conclude that the difference in the overall shape and size of both solvent molecules would lead to a less efficient packing, that is, a more straightforward release, of the *n*-heptane molecules in the intermicellar domain. Note that this observation is also supported by experimental results previously obtained by our group using the DLS technique.[13]

4. CONCLUSION

We have presented a complementary analysis of structural and dynamical characteristics of water/BHDC RMs in pure benzene, at $W_0 = 5$ and $W_0 = 10$. Concerning the overall shape of the RMs, we obtained eccentricity values close to ~0.9, confirming that the BHDC RMs can be roughly pictured as ellipsoidal moieties. Despite the lack of spherical symmetries it is still possible to establish a reasonable linear relationship between hydrodynamic radii and W_0.

With regard to surface properties, we found that the accessible surface area values reveal a non-negligible contact between the inner water pool and the external nonpolar solvent. Moreover, this contact increases with W_0, most likely due to the gradual loss of structure of the interface which, in turn, would favor the penetration of water and benzene within the micellar interface domain.

The density profiles show the existence of three spatial domains within the RMs: an inner pool, the surfactant interface, and the external solvent. Some important observations are worth commenting: (i) in both RMs, water densities in the core are about ~80% of the bulk value; (ii) local concentration fluctuations at the interface of the $W_0 = 10$ RM are more marked, indicating the presence of less structured interfacial environments; (iii) the larger penetration of the external solvent into the micellar interface is manifested by a significant overlap between the density profiles of the surfactant tails, the water, and the benzene molecules; (iv) methyl moieties of the surfactant headgroups are oriented toward the water micellar core, whereas the benzyl groups lie closer to the surfactant chains and the nonpolar solvent molecules.

The degree of hydration of the BHDC headgroups also increases with W_0. Differences between the effective ion−water electrostatic interactions can be monitored by inspecting pair density profiles. In this context the first peak for the nitrogen−water oxygen profile is less intense and wider than the one for chloride−water oxygen pair.

The confinement affects the dynamical properties of water, the characteristic time scales of which appear to be significantly stretched. Combined effects derived from electrostatic and confining forces make the slowdown more marked, the smaller the micellar size considered.

With regard to the coalescence process, we observed important modifications in the corresponding free energy profiles, depending on the overall molecular geometry of the external nonpolar solvent. In particular, the more open arrangement of the *n*-heptane molecules facilitates the removal of solvent species in the intermicellar region, leading to an overall reduction in the local free energy barriers controlling the association process.

■ ASSOCIATED CONTENT

Supporting Information

Section 1: System Preparation Procedure. Section 2: Mathematical Proof: Hydrodynamics Radius vs W_0 for ellipsoid RMs This material is available free of charge via the Internet at http://pubs.acs.org/.

■ AUTHOR INFORMATION

Corresponding Author

*(J.R.) E-mail: javier@speedy.cnea.gov.ar. Tel: 54-11-6772-7046. Fax: 54-11-6772-7121.

Notes

The authors declare no competing financial interest.

■ ACKNOWLEDGMENTS

We gratefully acknowledge the financial support for this work by the Consejo Nacional de Investigaciones Científicas y Técnicas (CONICET, PIP 112-201101-00204), Agencia Nacional de Promoción Científica y Técnica (PICT 2012-0232), y Secretaría de Ciencia y Técnica de la Universidad Nacional de Río Cuarto. N.M.C. and J.R. hold research positions at CONICET. F.M.A thanks CONICET for a research fellowship.

■ REFERENCES

(1) Hoar, T. P.; Schulman, J. H. Transparent water-in-oil dispersions: the oleopathic hydro-micelle. *Nature* **1943**, *152*, 102−103.

(2) Paul, B. K.; Moulik, S. P. Uses and applications of micro-emulsions. *Curr. Sci.* **2001**, *80*, 990−1001.

(3) Dwars, T.; Paetzold, E.; Oehme, G. Reactions in micellar systems. *Angew. Chem., Int. Ed.* **2005**, *44*, 7174−99.
(4) Correa, N. M.; Biasutti, M. A.; Silber, J. J. Micropolarity of reversed micelles: comparison between anionic, cationic, and nonionic reversed micelles. *J. Colloid Interface Sci.* **1996**, *184*, 570−578.
(5) Correa, N. M.; Silber, J. J.; Riter, R. E.; Levinger, N. E. Nonaqueous polar solvents in reverse micelle systems. *Chem. Rev.* **2012**, *112*, 4569−4602.
(6) Shrestha, L. K.; Shrestha, R. G.; Aramaki, K.; Yoshikawa, G.; Ariga, K. Demonstration of solvent-induced one-dimensional nonionic reverse micelle growth. *J. Phys. Chem. Lett.* **2013**, *4*, 2585−2590.
(7) Corbeil, E. M.; Levinger, N. E. Dynamics of polar solvation in quaternary microemulsions. *Langmuir* **2003**, *19*, 7264−7270.
(8) Dokter, A. M.; Woutersen, S.; Bakker, H. J. Ultrafast dynamics of water in cationic micelles. *J. Chem. Phys.* **2007**, *126*, 124507.
(9) Klíčová, L.; Šebej, P.; Štacko, P.; Filippov, S. K.; Bogomolova, A.; Padilla, M.; Klán, P. CTAB/water/chloroform reverse micelles: a closed or open association model? *Langmuir* **2012**, *28*, 15185−15192.
(10) McNeil, R.; Thomas, J. K. Benzylhexadecyldimethylammonium chloride in microemulsions and micelles. *J. Colloid Interface Sci.* **1981**, *83*, 57−65.
(11) Jada, A.; Lang, J.; Zana, R.; Makhloufi, R.; Hirsch, E.; Candau, S. J. Ternary water in oil microemulsions made of cationic surfactants, water, and aromatic solvents. 2. Droplet sizes and interactions and exchange of material between droplets. *J. Phys. Chem.* **1990**, *94*, 387−395.
(12) Quintana, S. S.; Moyano, F.; Falcone, R. D.; Silber, J. J.; Correa, N. M. Characterization of multifunctional reverse micelles interfaces using hemicyanines as molecular probes. II: Effect of the surfactant. *J. Phys. Chem. B* **2009**, *113*, 6718−6724.
(13) Agazzi, F. M.; Falcone, R. D.; Silber, J. J.; Correa, N. M. Solvent blends can control cationic reversed micellar interdroplet interactions. The effect of *n*-heptane:benzene mixture on BHDC reversed micellar interfacial properties: droplet sizes and micropolarity. *J. Phys. Chem. B* **2011**, *115*, 12076−12084.
(14) Agazzi, F. M.; Rodriguez, J.; Falcone, R. D.; Silber, J. J.; Correa, N. M. PRODAN dual emission feature to monitor BHDC interfacial properties changes with the external organic solvent composition. *Langmuir* **2013**, *29*, 3556−3566.
(15) Bagwe, R. P.; Khilar, K. C. Effects of the intermicellar exchange rate and cations on the size of silver chloride nanoparticles formed in reverse micelles of AOT. *Langmuir* **1997**, *13*, 6432−6438.
(16) Eastoe, J.; Hollamby, M. J.; Hudson, L. Recent advances in nanoparticle synthesis with reversed micelles. *Adv. Colloid Interface Sci.* **2006**, *128−130*, 5−15.
(17) Solanki, J. N.; Murthy, Z. V. P. Controlled size silver nanoparticles synthesis with water-in-oil microemulsion method: a topical review. *Ind. Eng. Chem. Res.* **2011**, *50*, 12311−12323.
(18) Khadzhiev, S. N.; Kadiev, K. M.; Yampolskaya, G. P.; Kadieva, M. K. Trends in the synthesis of metal oxide nanoparticles through reverse microemulsions in hydrocarbon media. *Adv. Colloid Interface Sci.* **2013**, *197−198*, 132−145.
(19) Gutierrez, J. A.; Falcone, R. D.; Lopez-Quintela, M. A.; Buceta, D.; Silber, J. J.; Correa, N. M. On the investigation of the droplet-droplet interactions of sodium 1,4-bis(2-ethylhexyl) sulfosuccinate reverse micelles upon changing the external solvent composition and their impact on gold nanoparticle synthesis. *Eur. J. Inorg. Chem.* **2014**, *2014*, 2095−2102.
(20) Brunetti, S.; Roux, D.; Bellocq, A. M.; Fourche, G.; Bothorel, P.; Dorshow, R. B.; Bunton, C. A.; Nicoli, D. F.; Lemaire, B. Micellar interactions in water-in-oil microemulsions. 1. Calculated interaction potential. *J. Phys. Chem.* **1983**, *87*, 1409−1416.
(21) Bouaskarne, M.; Amokrane, S.; Regnaut, C. Effective interaction between reverse micelles: a study from the potential of mean force at infinite dilution. *J. Chem. Phys.* **2001**, *114*, 2442.
(22) Gazzillo, D.; Giacometti, A.; Fantoni, R.; Sollich, P. Multi-component adhesive hard sphere models and short-ranged attractive interactions in colloidal or micellar solutions. *Phys. Rev. E* **2006**, *74*, No. 051407.
(23) Salabat, A.; Eastoe, J.; Mutch, K. J.; Tabor, R. F. Tuning aggregation of microemulsion droplets and silica nanoparticles using solvent mixtures. *J. Colloid Interface Sci.* **2008**, *318*, 244−251.
(24) McPhee, J. T.; Scott, E.; Levinger, N. E.; Van Orden, A. Cy3 in AOT reverse micelles II. Probing intermicellar interactions using fluorescence correlation spectroscopy. *J. Phys. Chem. B* **2011**, *115*, 9585−9592.
(25) Sharma, S.; Pal, N.; Chowdhury, P. K.; Sen, S.; Ganguli, A. K. Understanding growth kinetics of nanorods in microemulsion: a combined fluorescence correlation spectroscopy, dynamic light scattering, and electron microscopy study. *J. Am. Chem. Soc.* **2012**, *134*, 19677−19684.
(26) Abel, S.; Waks, M.; Marchi, M.; Urbach, W. Effect of surfactant conformation on the structures of small size nonionic reverse micelles:? A molecular dynamics simulation study. *Langmuir* **2006**, *22*, 9112−9120.
(27) Rodriguez, J.; Mart, J.; Gurdia, E.; Laria, D. Protons in non−ionic aqueous reverse micelles. *J. Phys. Chem. B* **2007**, *111*, 4432−4439.
(28) Rodriguez, J.; Laria, D.; Guardia, E.; Marti, J. Dynamics of water nanodroplets and aqueous protons in non-ionic reverse micelles. *Phys. Chem. Chem. Phys.* **2009**, *11*, 1484−1490.
(29) Guchhait, B.; Biswas, R.; Ghorai, P. K. Solute and solvent dynamics in confined equal-sized aqueous environments of charged and neutral reverse micelles: a combined dynamic fluorescence and all-atom molecular dynamics simulation study. *J. Phys. Chem. B* **2013**, *117*, 3345−3361.
(30) Faeder, J.; Ladanyi, B. M. Molecular dynamics simulations of the interior of aqueous reverse micelles. *J. Phys. Chem. B* **2000**, *104*, 1033−1046.
(31) Faeder, J.; Ladanyi, B. M. Solvation dynamics in reverse micelles: the role of headgroup−solute interactions. *J. Phys. Chem. B* **2005**, *109*, 6732−6740.
(32) Abel, S.; Sterpone, F.; Bandyopadhyay, S.; Marchi, M. Molecular modeling and simulations of AOT-water reverse micelles in isooctane:? Structural and dynamic properties. *J. Phys. Chem. B* **2004**, *108*, 19458−19466.
(33) Mudzhikova, G.; Brodskaya, E. Molecular simulation of an aerosol OT reverse micelle: 1. The shape and structure of a micelle. *Colloid J.* **2006**, *68*, 729−737.
(34) Brodskaya, E. N.; Mudzhikova, G. V. Molecular dynamics simulation of AOT reverse micelles. *Mol. Phys.* **2006**, *104*, 3635−3643.
(35) Mudzhikova, G. V.; Brodskaya, E. N. Molecular simulation of an aerosol OT reverse micelle: 2. Energy and kinetic characteristics. *Colloid J.* **2006**, *68*, 738−742.
(36) Chowdhary, J.; Ladanyi, B. M. Molecular dynamics simulation of aerosol-OT reverse micelles. *J. Phys. Chem. B* **2009**, *113*, 15029−15039.
(37) Chowdhary, J.; Ladanyi, B. M. Molecular simulation study of water mobility in aerosol-OT reverse micelles. *J. Phys. Chem. A* **2011**, *115*, 6306−6316.
(38) Vasquez, V. R.; Williams, B. C.; Graeve, O. A. Stability and comparative analysis of AOT/water/isooctane reverse micelle system using dynamic light scattering and molecular dynamics. *J. Phys. Chem. B* **2011**, *115*, 2979−2987.
(39) Martinez, A. V.; Dominguez, L.; Malolepsza, E.; Moser, A.; Ziegler, Z.; Straub, J. E. Probing the structure and dynamics of confined water in AOT reverse micelles. *J. Phys. Chem. B* **2013**, *117*, 7345−7351.
(40) MacKerell, A. D.; Banavali, N.; Foloppe, N. Development and current status of the CHARMM force field for nucleic acids. *Biopolymers* **2000**, *56*, 257−265.
(41) Berendsen, H. J. C.; Grigera, J. R.; Straatsma, T. P. The missing term in effective pair potentials. *J. Phys. Chem.* **1987**, *91*, 6269−6271.
(42) Mark, P.; Nilsson, L. Structure and dynamics of the TIP3P, SPC, and SPC/E water models at 298 K. *J. Phys. Chem. A* **2001**, *105*, 9954−9960.
(43) Smith, G. D.; Jaffe, R. L. Comparative study of force fields for benzene. *J. Phys. Chem.* **1996**, *100*, 9624−9630.

(44) Phillips, J. C.; Braun, R.; Wang, W.; Gumbart, J.; Tajkhorshid, E.; Villa, E.; Chipot, C.; Skeel, R. D.; Kalé, L.; Schulten, K. Scalable molecular dynamics with NAMD. *J. Comput. Chem.* **2005**, *26*, 1781−1802.
(45) Darden, T.; York, D.; Pedersen, L. Particle mesh Ewald: an Nlog(N) method for Ewald sums in large systems. *J. Chem. Phys.* **1993**, *98*, 10089−10092.
(46) Essmann, U.; Perera, L.; Berkowitz, M. L.; Darden, T.; Lee, H.; Pedersen, L. G. A smooth particle mesh Ewald method. *J. Chem. Phys.* **1995**, *103*, 8577−8593.
(47) Henin, J.; Chipot, C. Overcoming free energy barriers using unconstrained molecular dynamics simulations. *J. Chem. Phys.* **2004**, *121*, 2904−2914.
(48) Pomata, M. H. H.; Laria, D.; Skaf, M. S.; Elola, M. D. Molecular dynamics simulations of AOT-water/formamide reverse micelles: structural and dynamical properties. *J. Chem. Phys.* **2008**, *129*, 2445031−2445039.
(49) Kotlatchyk, M.; Chen, S.-H. Temperature dependence of size and polydispersity in a three-component microemulsion by small−angle neutron scattering. *J. Phys. Chem.* **1982**, *86*, 3273−3276.
(50) Masuya, M. NSOL-a numerical calculation program of molecular surface area, volume, and solvation energy. 2003; http://biocomputing.cc/nsol.
(51) Powell, D. H.; Neilson, G. W.; Enderby, J. E. The structure of Cl^- in aqueous solution: an experimental determination of $g_{ClH}(r)$ and $g_{ClO}(r)$. *J. Phys.−Condens. Mater.* **1993**, *5*, 5723.
(52) Enderby, J. E. Ion solvation via neutron scattering. *Chem. Soc. Rev.* **1995**, *24*, 159−168.
(53) Nevidimov, A. V.; Razumov, V. F. Molecular dynamics simulations of AOT reverse micelles' self-assembly. *Mol. Phys.* **2009**, *107*, 2169−2180.
(54) Gardner, A.; Vásquez, V.; Clifton, A.; Graeve, O. Molecular dynamics analysis of the AOT/water/isooctane system: effect of simulation time, initial configuration, and model salts. *Fluid Phase Equilib.* **2007**, *262*, 264−270.
(55) Bakulin, A. A.; Cringus, D.; Pieniazek, P. A.; Skinner, J. L.; Jansen, T. L. C.; Pshenichnikov, M. S. Dynamics of water confined in reversed micelles: multidimensional vibrational spectroscopy study. *J. Phys. Chem. B* **2013**, *117*, 15545−15558.
(56) Luzar, A.; Chandler, D. Hydrogen−bond kinetics in liquid water. *Nature* **1996**, *379*, 55−57.
(57) Elola, M. D.; Ladanyi, B. M. Computational study of structural and dynamical properties of formamide-water mixtures. *J. Chem. Phys.* **2006**, *125*, 184506.
(58) Rosenfeld, D. E.; Schmuttenmaer, C. A. Dynamics of the water hydrogen bond network at ionic, nonionic, and hydrophobic interfaces in nanopores and reverse micelles. *J. Phys. Chem. B* **2011**, *115*, 1021−1031.
(59) Chowdhary, J.; Ladanyi, B. M. Hydrogen bond dynamics at the water/hydrocarbon interface. *J. Phys. Chem. B* **2009**, *113*, 4045−4053.
(60) Laage, D.; Hynes, J. T. Reorientional dynamics of water molecules in anionic hydration shells. *Proc. Natl. Acad. Sci. U.S.A.* **2007**, *104*, 11167−11172.